Carcinogenesis, 2020, Vol. 41, No. 8, 1123–1133

doi:10.1093/carcin/bgz188
Advance Access Publication November 19, 2019
Original Article

ORIGINAL ARTICLE

Knockdown of ISOC1 inhibits the proliferation and migration and induces the apoptosis of colon cancer cells through the AKT/GSK-3β pathway

Bo Gao[1], LianMei Zhao[2], FeiFei Wang[1], HanYu Bai[2], Jing Li[1], Meng Li[1], XuHua Hu[1], Jian Cao[1], and GuiYing Wang[1,3,*]

[1]The Second General Surgery, The Fourth Hospital of Hebei Medical University, Shijiazhuang 050000, China, [2]Scientific Research Center, The Fourth Hospital of Hebei Medical University, Shijiazhuang 050000, China and [3]Department of General Surgery, The Third Hospital of Hebei Medical University, Shijiazhuang 050000, China

*To whom correspondence should be addressed. Tel: +86 0311 86095347; Fax: +86 0311 86032788; Email: wangguiyingtgzy@163.com

Abstract

Isochorismatase domain-containing 1 (ISOC1) is a coding gene that contains an isochorismatase domain. The precise functions of ISOC1 in humans have not been clarified; however, studies have speculated that it may be involved in unknown metabolic pathways. Currently, it is reported that ISOC1 is associated with breast cancer. In this research, the aim is to investigate the critical role of ISOC1 in colorectal cancer (CRC) and to explore its biological function and mechanism in colon cancer cells. In 106 paired clinical samples, we found that the levels of ISOC1 expression were widely increased in cancer tissues compared with matched adjacent non-tumor tissues and that increased expression of ISOC1 was significantly associated with tumor size, tumor invasion, local lymph node metastasis and Tumor, Node and Metastasis (TNM) stage. Moreover, higher expression levels of ISOC1 were correlated with shorter disease-free survival in patients 2 years after surgery. *In vitro*, ISOC1 knockdown inhibited the proliferation and migration and induced the apoptosis of colon cancer cells, and *in vivo*, the xenograft tumors were also inhibited by ISOC1 silencing. We also used MTS, Transwell and cell apoptosis assays to confirm that ISOC1 plays a critical role in regulating the biological functions of colon cancer cells through the AKT/GSK-3β pathway. Additionally, the results of confocal microscopy and western blot analysis indicated that ISOC1 knockdown could promote p-STAT1 translocation to the nucleus.

Introduction

Global cancer statistics estimates for 2018 showed that colorectal cancer (CRC) was the third most commonly diagnosed cancer and the second leading cause of cancer-related death (1). Clinical data showed that there was a higher proportion of patients with *de novo* metastatic disease, and even after chemotherapy, approximately 25–30% of patients with stage II/III disease had a recurrence within 5 years of surgery (2). CRC also has a high incidence in China (3). It is worth noting that the case-fatality ratio of CRC in China is 14%, which is higher than the global average of 12.2%, and the mortality/incidence ratio in China is 52.1%, which is higher than the global average of 48.3% (4). Therefore, we have to explore more effective treatment methods.

Isochorismatase domain-containing 1 (ISOC1), also known as CGI-111, is a protein-coding gene that belongs to the isochorismatase hydrolase family, along with its paralog ISOC2. Isochorismatase, also known as 2,3-dihydro-2,3-dihydroxybenzoate synthase, catalyzes the conversion of isochorismate, in the presence of water, to 2,3-dihydroxybenzoate and pyruvate (5). ISOC1 comprises 298 amino acids, and its chromosomal location is 5q23.3. Peroxisomes may be the major intracellular location of ISOC1. ISOC1 has been reported in some research: the expression level of ISOC1 was associated with progressive chronic renal failure in rats (6), with highly susceptible to *Staphylococcus aureus* in mice (7), and with early neutrophil

Received: February 12 2019; **Revised:** October 29 2019; **Accepted:** November 18 2019

Abbreviations

CRC	colorectal cancer
GTEx	Genotype-Tissue Expression
ISOC1	isochorismatase domain-containing 1
NC	negative control
TCGA	The Cancer Genome Atlas

development via targeting by miR-130a, which forms a complex with other target proteins to affect metabolism (8). There has been relatively little research on the role of ISOC1 in cancer; however, a tumor-related protein (gi14572526), which is homologous to ISOC1, was identified in the rat liver (9). As a multiple tumor suppressor, $p16^{INK4a}$ could be inhibited by overexpressing ISOC2, suggesting that, as another member of the same family as ISOC1, ISOC2 may play a role during tumor development (10). Previous studies have reported that the relationship between ISOC1 and tumors, including the expression of ISOC1 in leiomyoma, was significantly higher than that in normal myometrium (11), ISOC1 was more abundantly expressed in ERα-positive breast cancer tissues than in ERα-negative tissues (12), and ISOC1 knockdown impaired the growth of breast cancer cells (13). However, the role of ISOC1 in CRC is still unknown. The purpose of this study was to clarify the expression of ISOC1 in CRC and colon cancer cell lines and the role and potential mechanism of ISOC1 in colon cancer cells.

Materials and methods

Patients and tissue samples

Legally effective informed consent was obtained from all patients whose samples were used in this study, and ethics committee approval for this study was also obtained. In this study, all 106 patients with CRC eceived surgical treatment in the Second General Surgery of the Fourth Hospital of Hebei Medical University from July 2015 to October 2018. Patients with primary CRC in stages I–IV, based on the seventh edition of the American Joint Commission on Cancer Staging System (AJCC), and complete clinicopathologic data met the inclusion criteria. Patients who underwent preoperative radiotherapy, chemotherapy or biological therapy were excluded. All 106 paired CRC tissue samples included tumor tissue specimens (confirmed by pathological diagnosis) and matched adjacent non-tumor tissue specimens (at least 5 cm away from the edge of the tumor mass). Patients with a postoperative period of 24 months were followed up, and the data obtained were used for disease-free survival probability analysis.

Cell culture and drug treatment

NCM460, a healthy human colon mucosa cell line, was obtained from INCELL (San Antonio). HCT116, SW480, HT-29, RKO and DLD-1 human colon cancer cell lines were purchased (6–12 months prior to experiments) from Type Culture Collection of the Chinese Academy of Science (Shanghai, China). At the time of purchase, all cell lines were analyzed by the short tandem repeat STR method recommended by American Type Culture Collection (ATCC) to confirm the identity of the human cell lines and to rule out both intraspecies and interspecies contamination. Cells were maintained in RPMI 1640 medium and Dulbecco's modified Eagle's medium supplemented with 1% penicillin-streptomycin (Gibco) and 10% fetal bovine serum (Biological Industries, Israel) at 37°C in 5% CO_2. 7-Hydroxystaurosporine (UCN01) was purchased from Sigma (U6508), dissolved in dimethyl sulfoxide at 20 mM and then stored at –20°C.

RNA extraction and qRT–PCR

The RNA was extracted from frozen tissue samples and cultured cells using the TRIzol reagent (Invitrogen, Carlsbad, CA). Total RNA (1 μg) was reverse transcribed to single-stranded cDNA by using the Transcriptor First Strand cDNA Synthesis Kit (Roche, Germany) after examining the purity and concentration of the RNA. The cDNA was used as the template for the quantitative real-time PCR (qRT–PCR) with TransStart® Top Green qPCR SuperMix (TRANS®, Beijing). The application of primers was as follows: ISOC1 forward, 5′-AACAAACTGCCCTGGAGCTA-3′ and reverse, 5′-TCTGGAGCACTCGCCTTAAT-3′; GAPDH forward, 5′-CGGATTTGGTCGTATTGGG-3′ and reverse, 5′-TGCTGGAAGATGGTGATG GGATT-3′. All samples were run in triplicate, and the differences in ISOC1 mRNA expression were compared by using the $2^{-\Delta Ct}$ method.

Immunohistochemistry

The tissue specimens were fixed with formaldehyde and paraffin-embedded. Tissue sections cut from the paraffin blocks were dewaxed and then immersed in citrate buffer (0.01 M, pH 6.0), which was used for antigen retrieval. Endogenous peroxidase activity of the samples was inhibited using H_2O_2 (3%). Normal goat serum (5%) was used to block the heterogenetic antigens. Rabbit anti-ISOC1 polyclonal antibody (ab118245, Abcam) was used for staining. Goat anti-rabbit IgG polyclonal antibody (G23303, Servicebio, China) was used as the secondary antibody to bind the third antibody. Sections were stained with horseradish peroxidase-conjugated streptavidin working solution. The specimens were covered by DAB chromogen (Servicebio, China) for color development, counterstained with hematoxylin and mounted with neutral gum.

Immunostaining results were assessed independently by two pathologists. The intensity of staining was scored visually and recorded as –~+ for negative and as ++~+++ for positive.

Cell infection and transfection

The effective RNA interference ISOC1 target sequences 1 (5′-ATTTGAGTACCAGCATTTA-3′) and 2 (5′-CCAGAAGTAGAAGCGGCA TTA-3′) were designed by GeneChem Co., Ltd. The negative control (NC) had a non-targeting sequence (5′-TTCTCCGAACGTGTCACGT-3′). The short-hairpin structural RNA (shRNA) with the NC sequence (shCtrl) or the ISOC1-targeting sequences (shISOC1-1 and shISOC1-2) were inserted into the vector (Supplementary Material 1, available at *Carcinogenesis* Online), which stably expressed shRNA and a marker (EGFP). This vector was used to prepare lentivirus. Small interfering RNA targeting AKT and its phosphorylation site (AKT Thr^{308}) of deletion and activation plasmids were synthesized and purchased from GenePharma Co., Ltd and GeneChem Co., Ltd, respectively (Supplementary Materials 2 and 3, available at *Carcinogenesis* Online).

The cells were infected with lentivirus or transfected with small interfering RNA and plasmids, and the entire procedure followed the manufacturer's instructions (Supplementary Methods 1 and 2, available at *Carcinogenesis* Online). The infected cells with green fluorescence could be observed with fluorescence microscopy (Nikon Eclipse TE2000-U, Japan).

Western blot analysis

Equal amounts of the different protein samples were electrophoretically separated by using sodium dodecyl sulfate–polyacrylamide gel electrophoresis with a 10–12% gel and then transferred onto a PVDF membrane (Millipore). After blocking the membrane in a TBS solution with 5% fat-free milk, the membranes were incubated with primary antibodies. Goat anti-rabbit IgG (611-131-122, ROCKLAND) was used as the secondary antibody. The blots were visualized by an LI-COR Odyssey 9120 Infrared Imaging System (LI-COR Biosciences). The antibodies used for the western blotting included GAPDH (AP0063, Bioworld), ISOC1 (ab118245, Abcam), AKT1/2/3 (ET1609-51, Huabio, China), P-AKT Thr^{308} (AF3262, Affinity), P-GSK-3β Ser^{9} (AF2016, Affinity), P-STAT1 Tyr^{701} (AF6300, Affinity), PARP1 (13371-1-AP, Proteintech), Caspase-3 (9662, CST), Caspase-8 (GB-11594, Servicebio, China), Caspase-9 (GB-11053-1, Servicebio, China), c-Myc (5605s, CST), MMP2 (4022s, CST) and MMP9 (3852s, CST).

Cell growth and proliferation assays

Cell growth assays were performed using a Celigo Image Cytometer (Nexcelom) to monitor the growth of cell numbers. After infection, cells in the logarithmic growth phase were seeded in triplicate in 96-well plates with a density of 2000 cells/well. Then, the cell images were captured, and the number of cells was calculated once a day for 5 days. Finally, the cell growth over 5 days was plotted to create a growth curve.

An MTS assay was performed to examine the proliferation of HCT-116 and SW-480 cells. Briefly, cells were plated in 96-well plates at a density of 2000/well, and the absorbance at 492 nm (OD value) was detected after 1, 2, 3, 4 and 5 days with a microplate reader after treatment with MTS solution (20 μl/well). The experiment was repeated three times, and the ratio of the OD value (days 1–5) to the average value of the first day (cell viability) was calculated and plotted as MTS curves.

Clone-forming cell assay

The cells were seeded in six-well plates at a density of 2000 cells per well. After 10 days of cultivation, the cells were fixed with 4% paraformaldehyde and stained with Giemsa. Then, images of the cell plates were captured, and the colonies were counted; the experiment was repeated three times.

Caspase-3/7 activity assay and cell apoptosis analysis

The cells were seeded in a 96-well plate with 10^4 cells/well, with a blank control well without cells. Then, Caspase-Glo (G8091, Promega) was added to each well, shaken for 30 min and incubated for 2 h at room temperature. The Caspase-Glo 3/7 assay releases a substrate of luciferase after being cleaved by caspase-3 and -7. The substrate of luciferase results in a luminescent signal that can be detected by a Synergy 2 Multi-Mode Reader (BioTek).

Annexin V-APC (88-8007-72, eBioscience) was used for cell staining in the cell apoptosis assay. According to the manufacturer's instructions, the cells (≥5 × 10^5/well) were washed, digested and then resuspended using 200 μl 1× binding buffer. Then, 10 μl annexin V-APC was added to 200 μl cell suspension and incubated in the dark at room temperature for 10–15 min. Cell apoptosis analysis was detected by a Guava easyCyte HT cytometer (Millipore).

Wound healing assay and Transwell migration assay

After infection, the cells (5.0 × 10^5/well) were seeded in six-well plates. Cells were allowed to grow to ≥80% confluence, then a pipette tip (200 μl) was used to scrape the cell layer of each culture plate to create scratch wounds. To inhibit cell division, serum-free medium containing 1 mM mitomycin was used to replace the complete medium. Phase-contrast images of wound fields were obtained at 0, 24 and 48 h after scratching.

Transwell migration assays were also used to test cell mobility. The cells were seeded on a non-coated membrane located in the upper chamber of a well in 24-well plates. Media without serum was added to the upper chamber, whereas media with 10% fetal bovine serum was added to the lower chamber to act as a chemoattractant for cell migration. After 24 h of incubation, cells that had not migrated were on the upper surface of the membrane, whereas the cells on the other side of the membrane were stained with crystal violet. The number of cells in five random fields of view was counted. Both experiments were repeated three times.

Animal experiments

Male BALB/c nude mice were purchased (Beijing Vital River Laboratory Animal Technology Co., Ltd) and then fed by staff at the Experimental Animal Center of the Fourth Hospital of Hebei Medical University. Six-week-old mice were randomly assigned to two groups (n = 5) and were injected subcutaneously in their right flanks with 5 × 10^6 infected cells. Tumor size was measured two times a week from days 1 to 21 post-implantation. Twenty-one days after subcutaneous inoculation, all mice were killed, and their tumors were weighed. Tumor volume was calculated using the following formula: (length × width^2)/2. Animal experiments followed the USA National Institutes of Health Guidelines.

PathScan intracellular signaling array

PathScan was used to detect changes in key signaling molecules in signal pathways. After infection, HCT-116 cells were collected and lysed. The PathScan® Antibody Array Kit (Cell Signaling Technology, #14471) was used for detection, and the procedure was performed according to the manufacturer's instructions.

Nuclear and cytoplasmic protein extraction

For the extraction of nuclear and cytoplasmic protein, cells were treated with the NE-PER™ Nuclear and Cytoplasmic Extraction Reagents (Thermo, 78833) according to the manufacturer's instructions.

Immunocytochemistry and confocal microscopy

After infection, the cells were grown on coverslips, fixed with 4% paraformaldehyde and blocked with 10% fetal bovine serum. The coverslips were then incubated with the indicated antibodies overnight at 4°C and then incubated with goat anti-rabbit Cy3 secondary antibody (Wuhan Servicebio Technology, China) for 50 min. DNA was stained with 4′,6-diamidino-2-phenylindole (Wuhan Servicebio Technology). Coverslip images were collected using a laser confocal microscope (Nikon Eclipse TI, Japan).

Statistical analysis

Statistical analysis was performed using SPSS version 23.0 software. The mean ± SD was used to depict the experimental data. One-way analysis of variance, Student's t-tests, and the Wilcoxon signed rank test were performed for comparisons. Chi-square analyses were used to analyze categorical variables. The Kaplan–Meier method was used to estimate disease-free survival. A P-value < 0.05 was considered statistically significant, and all statistical tests were two sided.

Results

ISOC1 is a CRC-associated gene and was knocked down with high efficiency by shRNA lentivirus

Our results showed that, compared with those in the matched non-tumor tissues, the mRNA expression levels of ISOC1 in cancer tissues were significantly elevated (Figure 1A, P = 0.008). The cancer genome atlas (TCGA) and Genotype-Tissue Expression (GTEx) database also showed that ISOC1 expressed higher in CRC tissues than normal tissues (http://gepia.cancer-pku.cn/detail.php?gene=isoc1); as shown in Supplementary Figure 1, available at *Carcinogenesis* Online, the difference was statistically significant only in our data, but not in TCGA and GTEx data. The disease-free survival analysis was performed via the Kaplan–Meier method, which is based on the cutoff value determined using receiver operating characteristic curves. The results showed that higher ISOC1 expression levels in patients were correlated with shorter disease-free survival (Figure 1B). The median disease-free survival time for patients with CRC with high ISOC1 expression or low ISOC1 expression was 19.5 and 22.8 months, respectively. Immunohistochemical staining was used to compare the expression of ISOC1 proteins in 38 pairs of CRC tissues and matched adjacent non-tumor tissues. As summarized in Table 1, comparing the upregulated ISOC1 expression and clinical-pathological features of 106 CRC cases showed that elevated ISOC1 expression was significantly associated with tumor size, tumor invasion, local lymph node metastasis and Tumor, Node and Metastasis (TNM) stage. As shown in Figure 1C, ISOC1 staining was predominantly positive in the cytoplasm of tumor cells, whereas weak staining of ISOC1 was present in non-tumor epithelial cells. The frequency of ISOC1 positive (++~+++) staining in CRC tissues (60.5%, 23 of 38 samples) was significantly higher (Supplementary Table, available at *Carcinogenesis* Online, χ^2 = 7.664, P = 0.006) than that in matched non-tumor tissues (28.9%, 11 of 38). Moreover, ISOC1 mRNA and protein expression were detected in NCM-460, HCT-116, SW-480, RKO, DLD-1 and HT-29 cell lines. In addition to the RKO cell line, the mRNA and protein expression of ISOC1 in the other colon cancer cell lines was higher than that in the normal colon epithelial cell line NCM460, as depicted in Figure 1D and E. The results also showed that the expression of ISOC1 was higher in the HCT-116 and SW-480 cells than in the other three colon cancer cell lines. Thus, HCT-116 and SW-480 were chosen for further experiments.

ISOC1 was downregulated in ISOC1-shRNA cell lines, and knockdown of ISOC1 inhibited colon cancer cell proliferation

To clarify the biological effect of ISOC1, we infected HCT-116 and SW-480 cell lines with the ISOC1-shRNA or NC lentivirus.

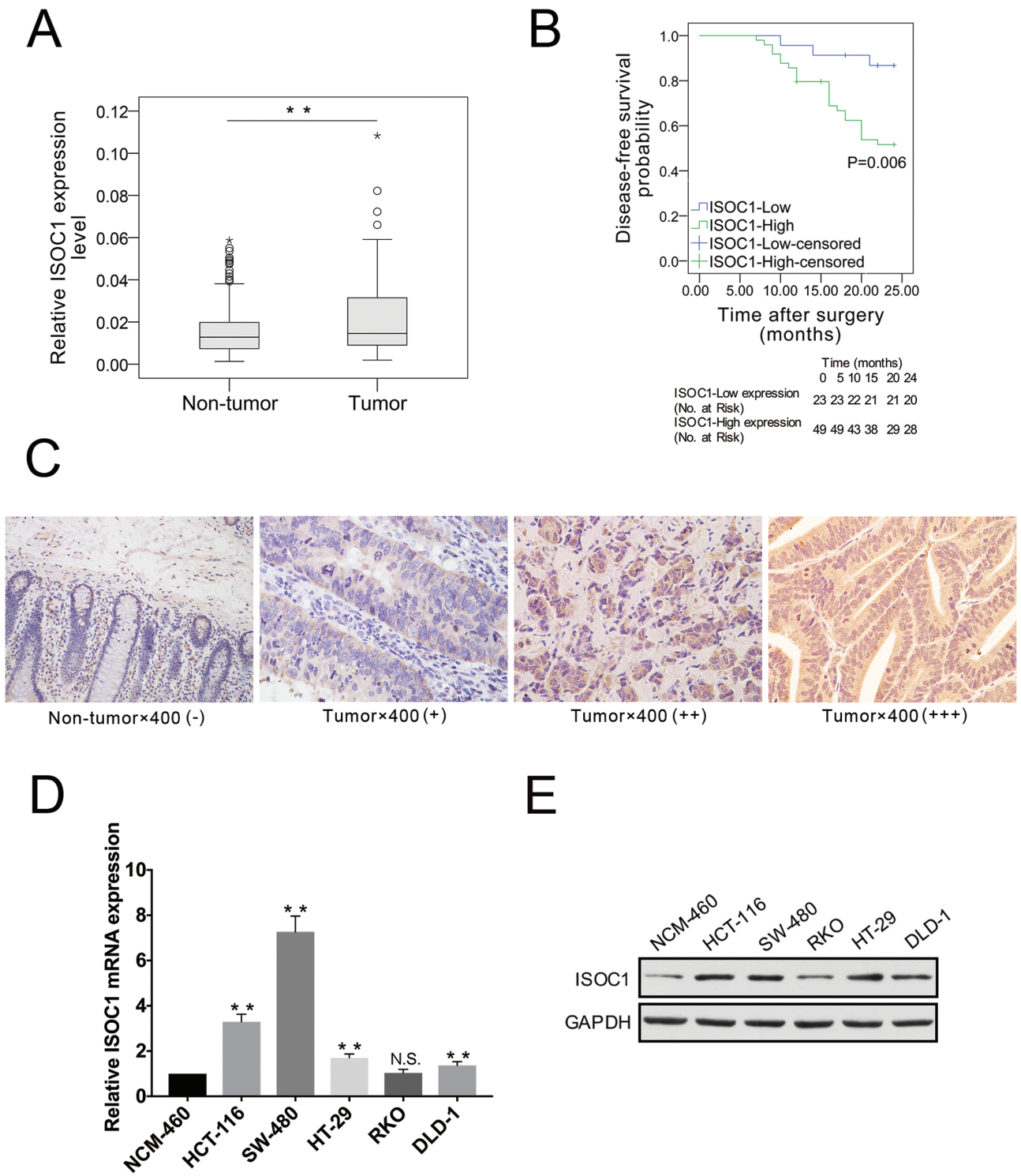

Figure 1. ISOC1 expression in ygjufikyfi samples NNNNNNNNNlk/0124528 cell lines. (**A**) ISOC1 expression was analyzed by qRT–PCR in 106 paired samples including tumor and adjacent non-tumor tissues. Statistical analysis was performed using the Wilcoxon signed ranks test, and the horizontal line indicates the median value. (**B**) The patient's 2-year disease-free survival (DFS) data, which were analyzed by the Kaplan–Meier method, were used to reflect the effect of the ISOC1 expression level on clinical prognosis. The survival probability of the ISOC1-high expression group (n = 49) was significantly lower than that of the ISOC1-low expression group (n = 23; log-rank test; P = 0.006). The cutoff threshold of ISOC1 expression is determined using the Youden index of receiver operating characteristic curves. (**C**) Representative immunohistochemistry staining of ISOC1 in CRC tissues and adjacent non-tumor tissues (×400). Negative: −~+; Positive: ++~+++. (**D**, **E**) ISOC1 mRNA and protein expression levels in colon cancer cell lines.

Approximately 72 h later, the percentage of cells with green fluorescence suggested infection efficiency is greater than approximately 80% (Supplementary Figure 2, available at *Carcinogenesis* Online). After approximately 72–120 h, the cells were harvested, and total proteins and RNAs were collected. The qRT–PCR results suggested that compared with that in

Table 1. Correlation between ISOC1 expression and clinicopathologic features in 106 CRC patients

Clinicopathologic features	ISOC1		χ^2	*P*-value
	Low	High		
All	53	53		
Age			0.151	0.697
≤62	27	29		
>62	26	24		
Gender			1.873	0.171
Male	23	20		
Female	16	19		
Tumor size			5.782	0.016*
≤5 cm	39	27		
>5 cm	14	26		
Tumor invasion			6.014	0.014*
T1 + T2	10	2		
T3 + T4	43	51		
N stage			6.526	0.011*
N0	37	24		
N1 + 2	16	29		
M stage			1.334	0.248
M0	52	0		
M1	50	3		
TNM stage			6.46	0.011*
+II	36	23		
III + IV	17	30		
Tumor embolus			0.07	0.791
Positive	8	9		
Negative	45	44		
Pathological differentiation			1.093	0.488
Well moderate	50	47		
Poor	3	6		

χ^2 tests were used to analyze the correlation between the expression level of ISOC1 and clinical features. The median expression level was used as the cutoff. Low expression of ISOC1 in 53 patients was classified as values below the 50th percentile. High ISOC1 expression in 53 patients was classified as values above the 50th percentile.
*$P < 0.05$ indicates the statistical significance.

the NC group (shCtrl group), the expression of ISOC1 in the knockdown groups (shISOC1-1 and shISOC1-2 groups) was reduced by approximately 75% in both cell lines. The results of the western blot assay showed that the protein level of ISOC1 was greatly reduced by infecting with ISOC1 shRNAs (Figure 2A). These results suggested effective knockdown of the target sequence occurred.

To explore whether ISOC1 can affect the proliferation of colon cancer cells, the infected HCT-116 cells were monitored by Celigo Image Cytometer. As shown in Figure 2B, compared with that of the NC group, the proliferation ability of the ISOC1 knockdown groups was obviously inhibited by day 5 of the observation period. The cell proliferation curve (cell count) and the curve of fold change (cell count/fold) were used to quantify the proliferation ability. After 5 days, the average number of cells in the ISOC1 knockdown groups was 3.21 times and 3.66 times that of the first day, compared with 7.38 times in the NC group.

The MTS assay was used to verify the effect of ISOC1 on proliferation. The results indicated that ISOC1 knockdown significantly reduced the proliferative activities of the HCT-116 and SW-480 cell lines. As shown in Figure 2C, the cell viability (OD492/fold) of the ISOC1 knockdown groups was significantly decreased compared with that of the NC group after culture for 4 days.

Furthermore, the results of the colony formation assay showed that ISOC1 knockdown induced a substantial reduction in the colony formation ability of HCT-116 and SW-480 cells (Figure 2D).

ISOC1 knockdown induced apoptosis in colon cancer cells

Caspase-3/7 activity and cell apoptosis assays were employed to investigate the effect of ISOC1 knockdown on apoptosis in colon cancer cells. As shown in Figure 3A, the relative caspase-3 and -7 activities were significantly higher in the ISOC1 knockdown groups than in the NC group. The results of the cell apoptosis assay suggested that the apoptosis rate of HCT-116 and SW-480 cells was dramatically increased in the ISOC1 knockdown groups compared with the NC group (Figure 3B). Based on the experiments shown here, ISOC1 may be related to the apoptosis of colon cancer cells. To explore the potential mechanism, the protein expression of PARP1 and caspase-3, -8 and -9 was examined. The results showed that, compared with that in the NC cells, the expression of cleaved PARP1 and cleaved caspase-3 and -9 in ISOC1 knockdown cells was increased, whereas the full lengths of these proteins were decreased. There was no significant difference in the expression of caspase-8 (Figure 3C).

The migration of colon cancer cells *in vitro* was inhibited by ISOC1 knockdown

The effect of ISOC1 on colon cancer cell migration was assessed by wound healing and Transwell migration assays. The results of the wound healing assay showed that, at 48 h after the scratch, HCT-116 or SW-480 cells that were NC lentivirus-infected almost completely closed the gap, whereas wounds were much slower to heal in cells infected with ISOC1-shRNA lentivirus (Figure 3D). The results of the Transwell migration assays suggested that after 24 h, the number of cells penetrating the membrane in the ISOC1 knockdown groups was significantly less than that in the NC group (Figure 3E). The wound healing and Transwell assays demonstrated that the migration capability of colon cancer cells was inhibited by ISOC1 silencing.

Knockdown of ISOC1 inhibited xenograft tumor growth *in vivo*

To investigate the effect of ISOC1 on the tumorigenicity of colon cancer cells *in vivo*, HCT-116 cells treated with ISOC1 shRNA (shISOC1-1) or NC lentivirus were subcutaneously implanted into nude mice (Supplementary Figure 3, available at *Carcinogenesis* Online). As shown in Figure 4A, the images showed that tumor growth was significantly decreased in the ISOC1 knockdown group, and the mean tumor volume and weight (Figure 4B and C) of the ISOC1 knockdown group were dramatically lower than those of the NC group. The expression of ISOC1 knockdown by shRNA was also confirmed by immunohistochemical experiments (Figure 4D).

Loss of ISOC1 affected the biological functions of colon cancer cells through the AKT/GSK-3β pathway and promoted the expression of p-STAT1 in the nucleus

To investigate the underlying signaling pathways mediated by ISOC1, the PathScan intracellular signaling array kit was utilized to detect 18 important signaling molecules in HCT-116 cell lines after ISOC1 knockdown (Figure 4E). The alterations that occurred in pivotal signaling proteins are shown in Figure 4F. The levels of cleaved PARP and caspase-3 and the levels of phosphorylated

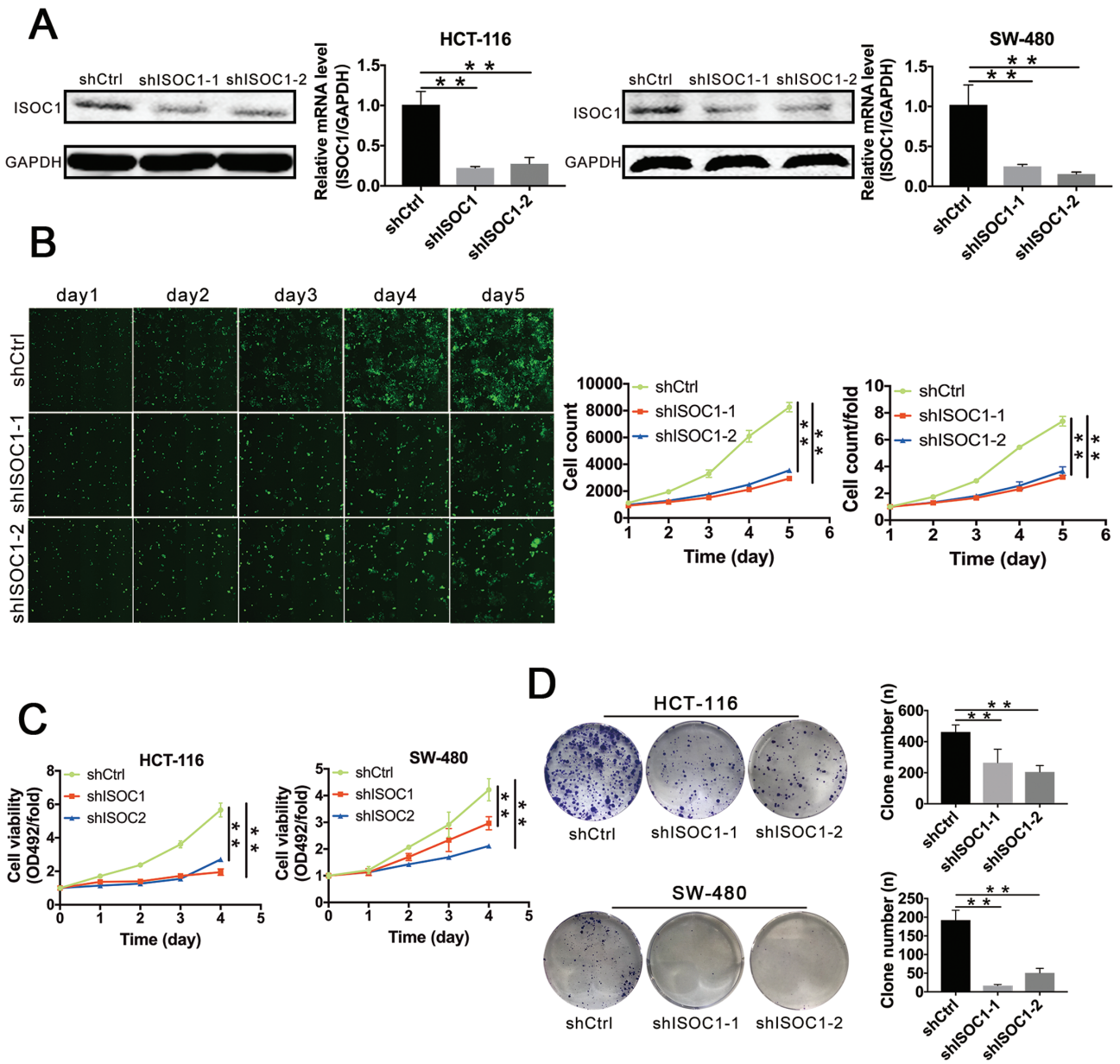

Figure 2. ISOC1 is downregulated in ISOC1-shRNA cell lines, and knockdown of ISOC1 inhibits colon cancer cell proliferation. (**A**) Knockdown efficiency of ISOC1 by shRNA lentivirus. Western blotting and qRT–PCR were performed to detect the ISOC1 expression levels in ISOC1 knockdown (shISOC1-1 and shISOC1-2) and negative control (shCtrl) cells. The error bars represent the standard deviation. *P < 0.05, **P < 0.01. (**B**) Cell growth assay. ISOC1 knockdown attenuated the growth potential of HCT-116 cells. The number of cells was counted every day for 5 days. The fold change of cell numbers on day 1 was set to 1 for normalization. (**C**) MTS assays. ISOC1 knockdown attenuated the cell viability (OD492/fold) of HCT-116 and SW-480 cells. (**D**) Colony formation assays. ISOC1 knockdown attenuated colony formation in HCT-116 and SW-480 cells. The error bars represent the standard deviation. *P < 0.05, **P < 0.01.

AKT Thr^{308}, GSK-3β Ser^{9}, STAT1 Tyr^{701} and AMP-activated protein kinase α Thr^{172} (AMPKα Thr^{172}) were obviously increased in ISOC1 knockdown cells compared with NC cells. The level of phosphorylated AKT Ser^{473} was not significantly increased.

Studies have shown that GSK-3β has tumor-promoting effects in colon cancer (14,15); however, GSK-3 activity was inhibited by phosphorylation at Ser^{9} of GSK-3β (16,17). Akt mediates the induction of an inactive form of GSK-3β by phosphorylating its Ser^{9} residue (18). Thus, we first determined the results of the PathScan array by using western blotting (Figure 4G). Then, we used UCN01, which can inhibit phosphorylation of AKT at Thr^{308} (19), to conduct mechanistic research in colon cancer cells. As shown in Figure 4H, after 20 min of treatment with UCN01, the protein levels of p-AKT at Thr^{308} in the ISOC1 knockdown cells decreased as the concentration of UCN01 increased. To reduce the effect of UCN01 alone on the experimental outcome, we administered UCN01 at the lowest possible effective dose of 100 nM. We also examined earlier time points and determined that there was a significant decrease in phospho-GSK-3β at Ser^{9} in the UCN01-treated cells after applying UCN01 for approximately 2 h (Figure 4I). Then, we divided the ISOC1 knockdown and NC group cells into four groups in the presence and absence of UCN01: shCtrl, shCtrl+UCN01, shISOC1, shISOC1 + UCN01. We further applied the MTS, Transwell and cell apoptosis assays

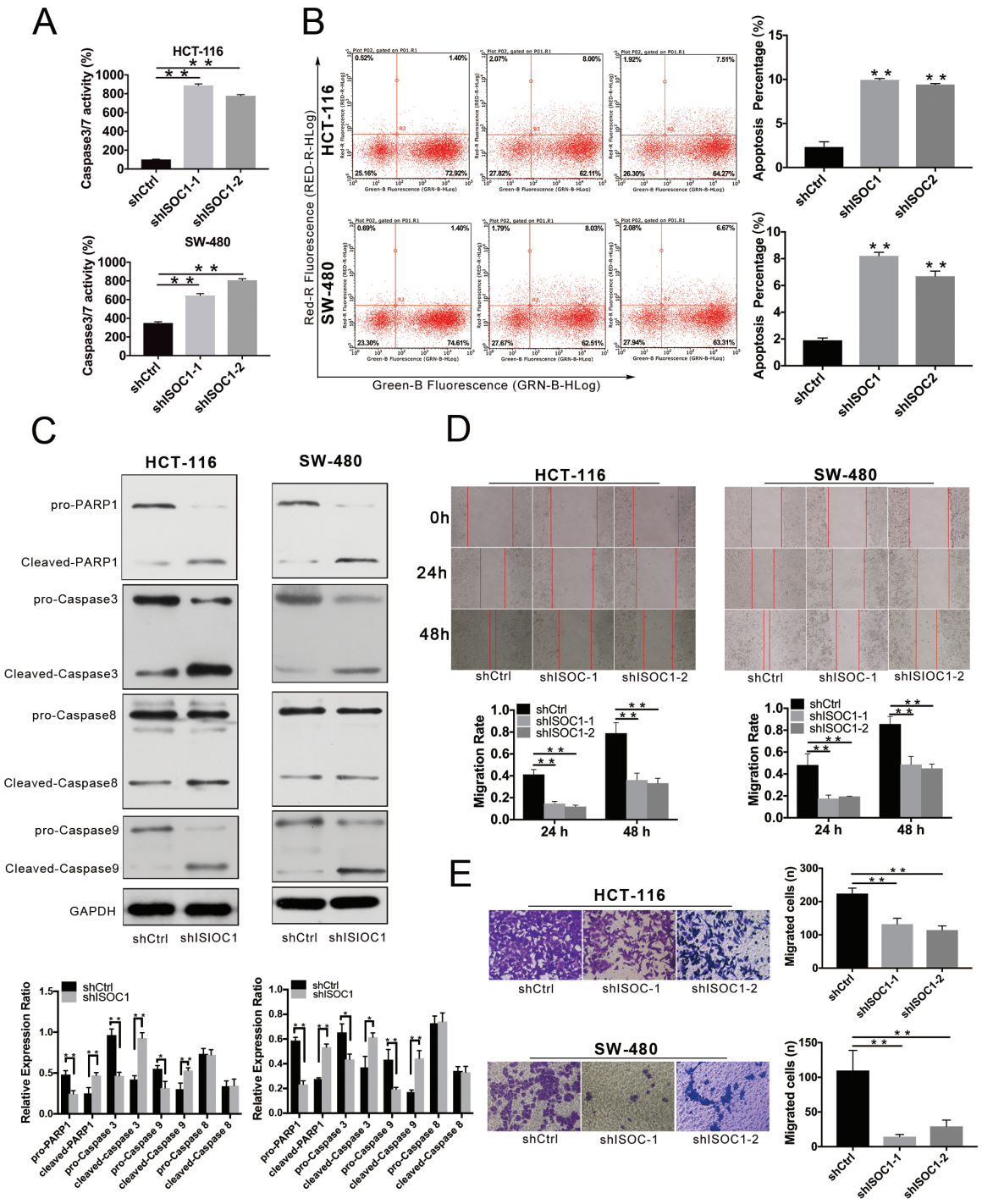

Figure 3. ISOC1 expression in CRC samples and cell lines. (**A**) Caspase-3/7 activity assay. Statistical analysis of caspase-3/7 activity in the shCtrl, shISOC1-1 and shISOC1-2 groups. (**B**) Cell apoptosis assay. Representative flow cytometric images in the shCtrl, shISOC1-1 and shISOC1-2 groups. (**C**) Western blot assay. The protein expression levels of cleaved PARP-1 and cleaved caspase-3 and -9 were increased in the shISOC1 (shISOC1-1) group compared with the shCtrl group, whereas the expression levels of pro-PARP-1 and pro-caspase-3 and -9 were decreased in the shISOC1 group compared with the shCtrl group. (**D**) Wound healing assay. The migration rate is derived from the ratio of the difference in wound width at different times to the initial wound width. (**E**) Transwell migration assays. The error bars represent the standard deviation. $^{*}P < 0.05$, $^{**}P < 0.01$.

(Figure 5A–C) to confirm the effect of ISOC1 on the biological behavior of colon cancer cells through the AKT/GSK-3β pathway. The proliferation, migration and apoptosis abilities of the ISOC1 knockdown cells were reversed after p-AKT Thr^{308} and p-GSK-3β Ser^{9} expression was suppressed with UCN01. At the same time, in the ISOC1 knockdown cells, we downregulated the mRNA and protein levels of AKT using small interfering RNA; however, the results of MTS (Supplementary Figure 4, available at *Carcinogenesis* Online) showed that downregulation of total AKT protein could not rescue the inhibition of colon cancer cell proliferation caused by ISOC1 silencing. Subsequently, we verified that the protein level of p-GSK-3β Ser^{9} could be upregulated

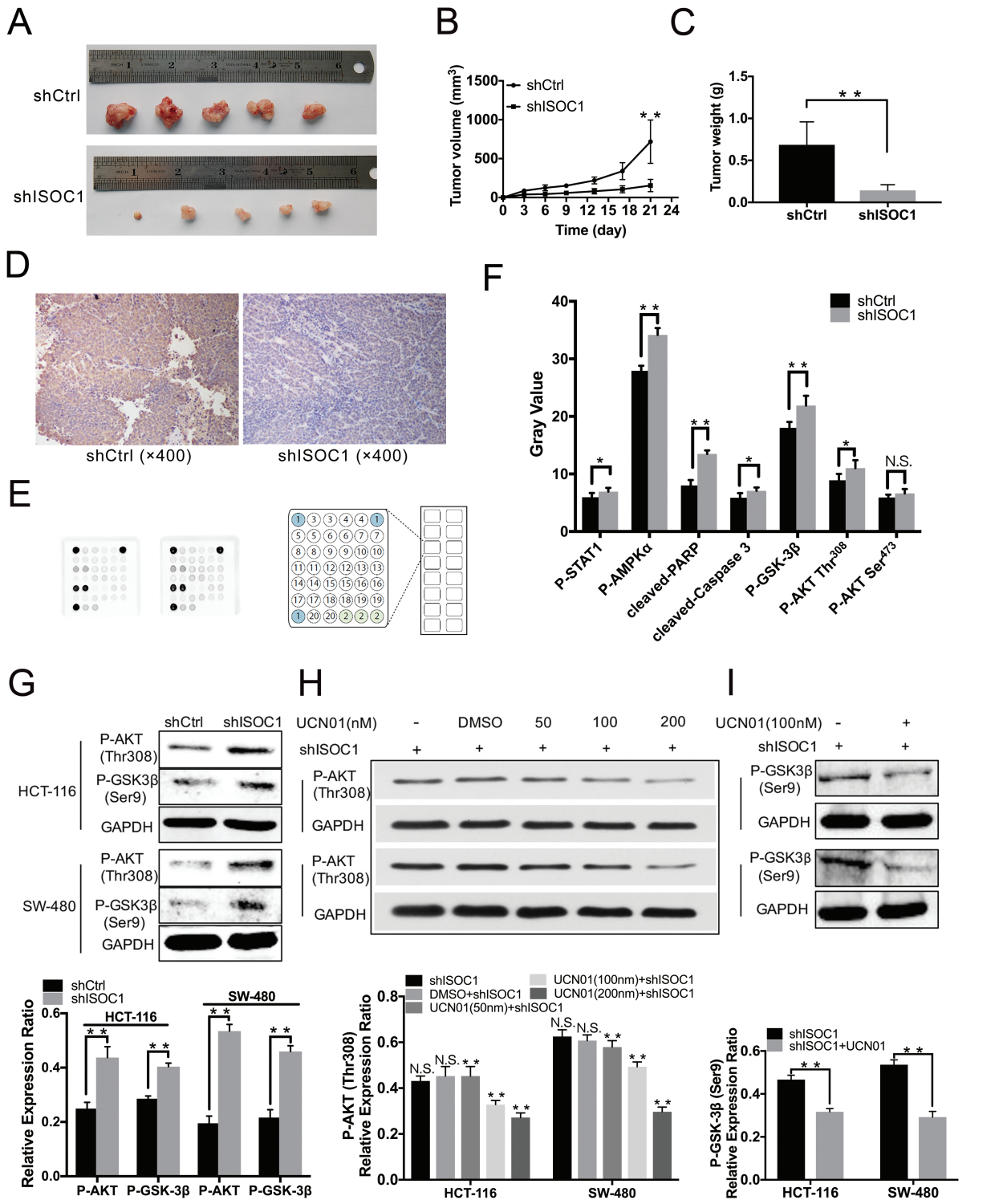

Figure 4. Knockdown of ISOC1 inhibits colon cancer cell growth *in vivo* and alters signaling proteins in colon cancer cells. (**A**) The tumors at day 21. HCT-116 cells infected with NC (shCtrl) or ISOC1-shRNA (shISOC1) lentivirus were subcutaneously implanted into nude mice, and 21 days later, the tumors were excised. (**B**) Tumor volumes were calculated in each group every 3 days from day 1 to day 21. (**C**) Tumor weights were measured on day 21. The error bars represent the standard deviation; $^{*}P < 0.05$, $^{**}P < 0.01$. (**D**) Representative immunohistochemical staining of ISOC1-shRNA (shISOC1) and NC (shCtrl) groups (×400). (**E**) PathScan assay. Eighteen pivotal signaling proteins were detected by the PathScan intracellular signaling array kit. (**F**) The upregulated proteins after silencing ISOC1. (**G**) Western blot assay. The protein levels of p-AKT Thr^{308} and p-GSK-3β Ser^{9} were increased in the shISOC1 group compared to the shCtrl group. (**H**, **I**) Western blot assay. The protein levels of p-AKT Thr^{308} and p-GSK-3β Ser^{9} decreased with UCN01 treatment (100/nM) in ISOC1 knockdown cells. The error bars represent the standard deviation. $^{*}P < 0.05$, $^{**}P < 0.01$.

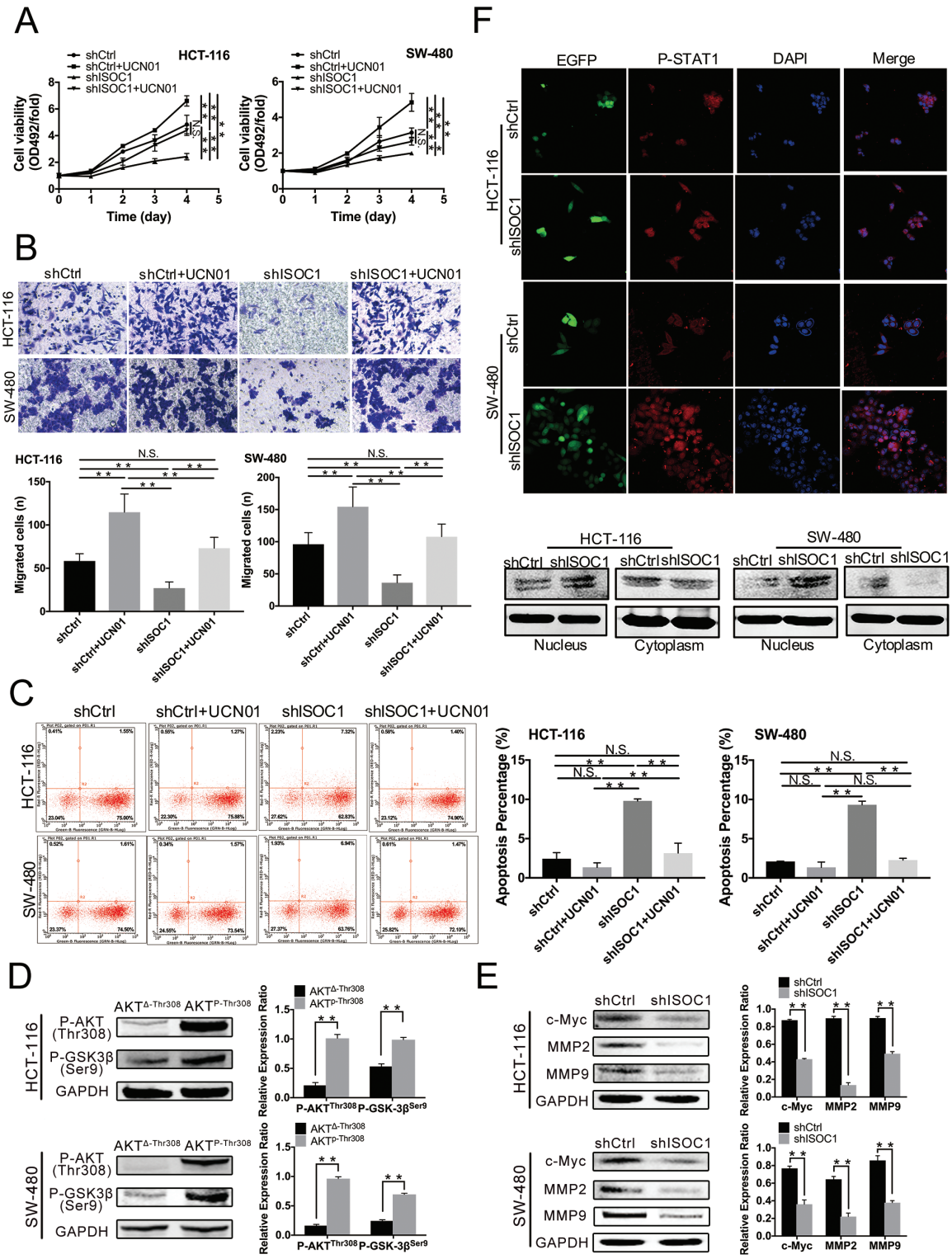

Figure 5. The effects of ISOC1 knockdown on the biological function of colon cancer cells are rescued by UCN01. Further verification of the mechanism of ISOC1 in colon cancer cells. The protein level of p-STAT Tyr^{701} in colon cancer cell nuclei was increased by ISOC1 knockdown. (**A**) MTS assays. (**B**) Transwell migration assays. (**C**) Cell apoptosis assay. (**D**) Western blot assay. The protein level of p-GSK-3β Ser^{9} was upregulated by overexpression of p-AKT Thr^{308}. AKT$^{\Delta\text{-Thr308}}$: p-AKT Thr^{308} deletion plasmid. AKT$^{\text{P-Thr308}}$: p-AKT Thr^{308} activation plasmid. (**E**) Western blot assay. The protein levels of c-Myc, MMP2 and MMP9 were significantly reduced by ISOC1 knockdown. (**F**) Confocal microscopy and western blot analysis of p-STAT1 Tyr^{701} nuclear localization. Green signals represent cells infected with lentiviruses. DNA was visualized with 4′,6-diamidino-2-phenylindole (DAPI) (blue). Western blot analysis showed that the protein levels of p-STAT1 Tyr^{701} were increased in the shISOC1 group compared to the shCtrl group. The error bars represent the standard deviation. *P < 0.05, **P < 0.01.

by overexpression of p-AKT Thr^{308} (Figure 5D). These results indicate that ISOC1 may affect colon cancer cells by partially activating AKT. To further explore the potential mechanism of ISOC1 knockdown effects on proliferation and migration, c-Myc, MMP2 and MMP9 protein levels were examined. As shown in Figure 5E, after downregulating ISOC1 in HCT-116 and SW-480 cells, the protein levels of c-Myc, MMP2 and MMP9 were significantly reduced.

STAT1 has been shown to have tumor-suppressive activity by inhibiting tumor angiogenesis, growth and metastasis (20). To investigate the effects of ISOC1 on STAT1, we examined the p-STAT1 Tyr^{701} protein level in ISOC1 knockdown HCT-116 and SW-480 cells. The western blotting results confirmed the observations made by immunofluorescence: compared with NC cells, ISOC1 knockdown obviously increased the levels of nuclear STAT1 protein (Figure 5F).

Discussion

CRC patients, even terminal cancer patients, have benefited from new advances over the past decade, including molecular characterization and application of targeted agents, etc (21). However, worldwide, CRC is still one of the highest ranked malignant tumors by morbidity and mortality rates. Researchers are attempting to search for novel molecular features and unravel the underlying mechanisms of cancer formation.

ISOC1 contains an isochorismatase domain that may be involved in the hydrolysis of ether bonds. The conversion of isochorismate to 2,3-dihydroxybenzoate and pyruvate is catalyzed by isochorismatase. Previously, this process was found to be a part of the shikimic acid pathway in microorganisms (22); however, ISOC1 and its homologs were also found in mammals (23,24). Thomas Gronemeyer *et al*. (23) reported five peroxisome-associated proteins in humans, including ISOC1, and further analysis may facilitate the discovery of new metabolic pathways. Reprogramming of energy metabolism is one of the 10 hallmarks of cancer (25), and studies (26–28) have also suggested that the diversity and complexity of metabolic mechanisms in cancer cells are beyond our understanding. It has been reported that cancer cells are able to increase glucose import into the cytoplasm, and most of the decomposed pyruvic acid is used for glycolysis in the cytoplasm (29–31). Aerobic glycolysis has also been reported for many years, indicating that even in an aerobic environment, cancer cellular energy is produced largely through glycolysis (25), and the intermediate product of glycolysis is likely to provide raw materials for assembling more new cells (32). Whether ISOC1 overexpression is involved in assembling more new cancer cells or in unknown energy metabolism mechanisms of cancer requires further study.

To better understand the role of ISOC1 in CRC, we conducted a preliminary study. Initially, we confirmed that compared with matched non-tumor tissues, ISOC1 expression was widely increased in cancer tissues and that the increased expression of ISOC1 was significantly associated with tumor size, tumor invasion, local lymph node metastasis and TNM stage. Then, patients were followed up for 2 years after the operation, and we found that higher expression levels of ISOC1 were correlated with shorter disease-free survival time. In addition, due to the small amount of transcriptome sequencing in normal CRC tissues in TCGA database, we combined TCGA and GTEx databases and obtained more data from them. In TCGA and GTEx database, we also found that the expression of ISOC1 in CRC tissues is higher than that in normal tissues, but it is not statistically significant. The difference between this result and our result may be due to the small sample size in the database or our experiments or the difference in the selected samples leading bias in the statistical results.

In the *in vitro* experiments, proliferation and migration were inhibited, and apoptosis was induced after ISOC1 knockdown in colon cancer cells. Furthermore, the xenograft tumors were also inhibited by ISOC1 silencing *in vivo*. We first explored how ISOC1 affects apoptosis-related proteins. The caspase family plays a central role in apoptosis (33), PARP is one of the first substrates that was shown to be cleaved by caspases (34,35), and the PARP1 protein contributes to 90% of the total cellular PARP activity (36). Our results showed that ISOC1 silencing may induce the apoptosis of colon cancer cells through the mitochondrial pathway.

As mentioned in the PathScan results, the expression of some key proteins in signaling pathways was increased after ISOC1 silencing; among these proteins, the role of AMPK in the tumor remains controversial (37). Phosphorylation of Akt at Thr^{308} leads to a substantial but incomplete activation of AKT (38,39), maximal activation requires additional phosphorylation at Ser^{473}; however, the protein level of p-AKT Ser^{473} was not significantly increased. As mentioned above, GSK-3β has tumor-promoting effects in colon cancer, Akt mediates inactivation of GSK-3β by phosphorylating its Ser^{9} residues, and the AKT inhibitor UCN01 inhibits phosphorylation of AKT at Thr^{308}. Thus, we used UCN01 to inhibit the activity of p-AKT Thr^{308} and GSK-3β Ser^{9} and confirmed that ISOC1 plays a critical role in colon cancer cells through the AKT/GSK-3β pathway by using MTS, Transwell and cell apoptosis assays. Additionally, in our study, downregulation of total AKT protein did not rescue the inhibition of colon cancer cell proliferation that was mediated by silencing of ISOC1. We speculate that this may be due to the partial activation of AKT caused by ISOC1 knockdown. To verify this, we overexpressed the protein level of p-AKT Thr^{308} in HCT-116 and SW-480 cell lines and found that the protein level of p-GSK-3β Ser^{9} increased significantly. To further explore the specific mechanism of ISOC1 on proliferation, apoptosis and migration of colon cancer cells, the protein levels of c-Myc, MMP2 and MMP9 were measured. C-Myc belongs to the MYC family, and its high expression is closely related to the growth and proliferation of cancer cells; it also participates in apoptosis resistance as a substrate for GSK-3β (40–42). MMP2 and MMP9 belong to the matrix metalloproteinase family and have important roles in cancer cell migration, invasion and metastasis (43,44). The results showed that the levels of the three proteins were significantly reduced after silencing ISOC1.

STAT1, which belongs to the STAT family, is a tumor suppressor gene (45,46), and the STAT1-containing complex can translocate to the nucleus to participate in cell proliferation, survival, apoptosis and differentiation. It requires phosphorylation at both Tyr^{701} and Ser^{727} for full activation (47). One study has reported that abrogation of STAT1 reversed antiproliferative effects in colon cancer cells (48). We found that silencing ISOC1 led to nuclear transposition of p-STAT1 Tyr^{701} in colon cancer cells, as revealed by confocal imaging and western blotting.

In conclusion, all of these results provide evidence that ISOC1 expression levels in CRC tissues are higher than those in matched non-tumor tissues. ISOC1 overexpression was associated with tumor size, tumor invasion, local lymph node metastasis and TNM stage. The higher expression of ISOC1 levels was correlated with shorter disease-free survival. ISOC1 was confirmed to play an important role in regulating colon cancer cell proliferation, migration and apoptosis through the AKT/GSK-3β pathway, and a high level of nuclear p-STAT1 Tyr^{701} was frequently found in ISOC1 knockdown cells of colon cancer. ISOC1 may be a prognostic factor and therapeutic target for CRC in the future.

Supplementary material

Supplementary data are available at *Carcinogenesis* online.

Funding

Natural Science Foundation of China (81502032, 81673642 and 81772550).

Acknowledgements

We wish to thank LianMei Zhao for help with the manuscript and the Experimental Animal Center of the Fourth Hospital of Hebei Medical University for help with animal experiments.

Conflict of Interest Statement: All of authors declare no potential conflicts of interest.

References

1. Bray, F. *et al.* (2018) Global cancer statistics 2018: GLOBOCAN estimates of incidence and mortality worldwide for 36 cancers in 185 countries. *CA. Cancer J. Clin.*, 68, 394–424.
2. Shah, M.A. *et al.* (2016) Impact of patient factors on recurrence risk and time dependency of oxaliplatin benefit in patients with colon cancer: analysis from modern-era adjuvant studies in the Adjuvant Colon Cancer End Points (ACCENT) Database. *J. Clin. Oncol.*, 34, 843–853.
3. Pan, R. *et al.*; China Kadoorie Biobank Collaborative Group. (2017) Cancer incidence and mortality: a cohort study in China, 2008–2013. *Int. J. Cancer*, 141, 1315–1323.
4. Zhu, J. *et al.* (2017) Epidemiological trends in colorectal cancer in China: an ecological study. *Dig. Dis. Sci.*, 62, 235–243.
5. Young, I.G. *et al.* (1969) Regulation of the enzymes involved in the biosynthesis of 2,3-dihydroxybenzoic acid in *Aerobacter aerogenes* and *Escherichia coli*. *Biochim. Biophys. Acta*, 177, 401–411.
6. Horiba, N. *et al.* (2004) Gene expression variance based on random sequencing in rat remnant kidney. *Kidney Int.*, 66, 29–45.
7. Ahn, S.H. *et al.* (2010) Two genes on A/J chromosome 18 are associated with susceptibility to *Staphylococcus aureus* infection by combined microarray and QTL analyses. *PLoS Pathog.*, 6, e1001088.
8. Pedersen, C.C. *et al.* (2015) Impact of microRNA-130a on the neutrophil proteome. *BMC Immunol.*, 16, 70.
9. Kikuchi, M. *et al.* (2004) Proteomic analysis of rat liver peroxisome: presence of peroxisome-specific isozyme of Lon protease. *J. Biol. Chem.*, 279, 421–428.
10. Huang, X. *et al.* (2007) Identification and characterization of a novel protein ISOC2 that interacts with p16INK4a. *Biochem. Biophys. Res. Commun.*, 361, 287–293.
11. Litovkin, K.V. *et al.* (2008) Microarray study of gene expression in uterine leiomyoma. *Exp. Oncol.*, 30, 106–111.
12. Rezaul, K. *et al.* (2010) Differential protein expression profiles in estrogen receptor-positive and -negative breast cancer tissues using label-free quantitative proteomics. *Genes Cancer*, 1, 251–271.
13. Yamaga, R. *et al.* (2014) Systemic identification of estrogen-regulated genes in breast cancer cells through cap analysis of gene expression mapping. *Biochem. Biophys. Res. Commun.*, 447, 531–536.
14. Shakoori, A. *et al.* (2007) Inhibition of GSK-3 beta activity attenuates proliferation of human colon cancer cells in rodents. *Cancer Sci.*, 98, 1388–1393.
15. Mai, W. *et al.* (2006) Detection of active fraction of glycogen synthase kinase 3beta in cancer cells by nonradioisotopic *in vitro* kinase assay. *Oncology*, 71, 297–305.
16. Harwood, A.J. (2001) Regulation of GSK-3: a cellular multiprocessor. *Cell*, 105, 821–824.
17. Beurel, E. *et al.* (2015) Glycogen synthase kinase-3 (GSK3): regulation, actions, and diseases. *Pharmacol. Ther.*, 148, 114–131.
18. Sharma, M. *et al.* (2002) Phosphatidylinositol 3-kinase/Akt stimulates androgen pathway through GSK3beta inhibition and nuclear beta-catenin accumulation. *J. Biol. Chem.*, 277, 30935–30941.
19. Kondapaka, S.B. *et al.* (2004) 7-Hydroxystaurosporine (UCN-01) inhibition of Akt Thr308 but not Ser473 phosphorylation: a basis for decreased insulin-stimulated glucose transport. *Clin. Cancer Res.*, 10, 7192–7198.
20. Huang, S. *et al.* (2002) Stat1 negatively regulates angiogenesis, tumorigenicity and metastasis of tumor cells. *Oncogene*, 21, 2504–2512.
21. Loree, J.M. *et al.* (2017) Recent developments in the treatment of metastatic colorectal cancer. *Ther. Adv. Med. Oncol.*, 9, 551–564.
22. Walsh, C.T. *et al.* (1990) Molecular studies on enzymes in chorismate metabolism and the enterobactin biosynthetic pathway. *Chem. Rev.*, 90, 1105–1129.
23. Gronemeyer, T. *et al.* (2013) The proteome of human liver peroxisomes: identification of five new peroxisomal constituents by a label-free quantitative proteomics survey. *PLoS One*, 8, e57395.
24. Islinger, M. *et al.* (2007) Rat liver peroxisomes after fibrate treatment. A survey using quantitative mass spectrometry. *J. Biol. Chem.*, 282, 23055–23069.
25. Hanahan, D. *et al.* (2011) Hallmarks of cancer: the next generation. *Cell*, 144, 646–674.
26. Locasale, J.W. *et al.* (2011) Phosphoglycerate dehydrogenase diverts glycolytic flux and contributes to oncogenesis. *Nat. Genet.*, 43, 869–874.
27. Chinnaiyan, P. *et al.* (2012) The metabolomic signature of malignant glioma reflects accelerated anabolic metabolism. *Cancer Res.*, 72, 5878–5888.
28. Ying, H. *et al.* (2012) Oncogenic Kras maintains pancreatic tumors through regulation of anabolic glucose metabolism. *Cell*, 149, 656–670.
29. DeBerardinis, R.J. *et al.* (2008) The biology of cancer: metabolic reprogramming fuels cell growth and proliferation. *Cell Metab.*, 7, 11–20.
30. Hsu, P.P. *et al.* (2008) Cancer cell metabolism: Warburg and beyond. *Cell*, 134, 703–707.
31. Jones, R.G. *et al.* (2009) Tumor suppressors and cell metabolism: a recipe for cancer growth. *Genes Dev.*, 23, 537–548.
32. Vander Heiden, M.G. *et al.* (2009) Understanding the Warburg effect: the metabolic requirements of cell proliferation. *Science*, 324, 1029–1033.
33. Rathmell, J.C. *et al.* (1999) The central effectors of cell death in the immune system. *Annu. Rev. Immunol.*, 17, 781–828.
34. Kaufmann, S.H. *et al.* (1993) Specific proteolytic cleavage of poly(ADP-ribose) polymerase: an early marker of chemotherapy-induced apoptosis. *Cancer Res.*, 53, 3976–3985.
35. Tewari, M. *et al.* (1995) Yama/CPP32 beta, a mammalian homolog of CED-3, is a CrmA-inhibitable protease that cleaves the death substrate poly(ADP-ribose) polymerase. *Cell*, 81, 801–809.
36. Drew, Y. *et al.* (2009) PARP inhibitors in cancer therapy: two modes of attack on the cancer cell widening the clinical applications. *Drug Resist. Updat.*, 12, 153–156.
37. Dasgupta, B. *et al.* (2016) Evolving lessons on the complex role of AMPK in normal physiology and cancer. *Trends Pharmacol. Sci.*, 37, 192–206.
38. Alessi, D.R. *et al.* (1997) Characterization of a 3-phosphoinositide-dependent protein kinase which phosphorylates and activates protein kinase Balpha. *Curr. Biol.*, 7, 261–269.
39. Alessi, D.R. *et al.* (1998) Mechanism of activation and function of protein kinase B. *Curr. Opin. Genet. Dev.*, 8, 55–62.
40. Rottmann, S. *et al.* (2005) A TRAIL receptor-dependent synthetic lethal relationship between MYC activation and GSK3beta/FBW7 loss of function. *Proc. Natl Acad. Sci. USA*, 102, 15195–15200.
41. Evan, G.I. *et al.* (1992) Induction of apoptosis in fibroblasts by c-myc protein. *Cell*, 69, 119–128.
42. Pelengaris, S. *et al.* (2002) c-MYC: more than just a matter of life and death. *Nat. Rev. Cancer*, 2, 764–776.
43. Gupta, G.P. *et al.* (2007) Mediators of vascular remodelling co-opted for sequential steps in lung metastasis. *Nature*, 446, 765–770.
44. Hiratsuka, S. *et al.* (2002) MMP9 induction by vascular endothelial growth factor receptor-1 is involved in lung-specific metastasis. *Cancer Cell*, 2, 289–300.
45. Stephanou, A. *et al.* (2005) Opposing actions of STAT-1 and STAT-3. *Growth Factors*, 23, 177–182.
46. Yu, H. *et al.* (2009) STATs in cancer inflammation and immunity: a leading role for STAT3. *Nat. Rev. Cancer*, 9, 798–809.
47. Ramsauer, K. *et al.* (2002) p38 MAPK enhances STAT1-dependent transcription independently of Ser-727 phosphorylation. *Proc. Natl Acad. Sci. USA*, 99, 12859–12864.
48. Elahi, A. *et al.* (2008) HPP1-mediated tumor suppression requires activation of STAT1 pathways. *Int. J. Cancer*, 122, 1567–1572.